Modelling and Measurement of a Moving Magnet Linear Compressor Performance

Kun Liang [a,*], Richard Stone [a], Gareth Davies [b], Mike Dadd [a], Paul Bailey [a]

[a] Department of Engineering Science, University of Oxford, Oxford OX1 3PJ, UK
[b] Centre for Air Conditioning and Refrigeration Research, London South Bank University, London SE1 0AA, UK
[*] *Corresponding author*. Tel: +44 1865 283093. Email address: kun.liang@eng.ox.ac.uk (K. Liang)

ABSTRACT

A novel moving magnet linear compressor with clearance seals and flexure bearings has been designed and constructed. It is suitable for a refrigeration system with a compact heat exchanger, such as would be needed for CPU cooling. The performance of the compressor has been experimentally evaluated with nitrogen and a mathematical model has been developed to evaluate the performance of the linear compressor. The results from the compressor model and the measurements have been compared in terms of cylinder pressure, the 'P-V' loop, stroke, mass flow rate and shaft power. The cylinder pressure was not measured directly but was derived from the compressor dynamics and the motor magnetic force characteristics. The comparisons indicate that the compressor model is well validated and can be used to study the performance of this type of compressor, to help with design optimization and the identification of key parameters affecting the system transients. The electrical and thermodynamic losses were also investigated, particularly for the design point (stroke of 13 mm and pressure ratio of 3.0), since a full understanding of these can lead to an increase in compressor efficiency.

Keywords: moving magnet linear compressor, mathematical model, measurements, P-V loop, losses

1. Introduction

1.1 Linear Compressor Development

Clearance seal pistons that are supported by flexure bearings are a well-established concept that was originally developed for Stirling cycle cryocoolers for use in space **[1]**; the absence of sliding parts leads to a long life. As has been indicated by Bradshaw et al. **[2]** and Bailey et al. **[3]**, the linear compressor is an attractive proposition for electronics cooling applications because it offers several benefits compared to traditional compressor technology. A linear compressor does not have a crank mechanism to drive the piston and is driven directly by a linear motor. The elimination of cranks and bearings significantly reduces the frictional losses associated with a conventional reciprocating compressor. Oil-free operation is possible, and this is a significant advantage with respect to the heat transfer performance of the condenser and the evaporator in a refrigeration system. In addition, the absence of oil widens both the choice of refrigerants and their operating temperature range. In a high efficiency linear machine, the piston operates resonantly in order to minimise the drive current. Resonance is determined by the moving mass and by the spring stiffness, which has two components: from the mechanical springs, and the 'gas spring' effect of the compression process.

One company that has been involved in these technologies over a long period is Sunpower. They have developed a system using linear gas bearings to support and maintain the alignment of the piston **[4, 5]**. Recent developments include a moving magnet designs in the Clever Fellows (Q drive) **[6]** and in the Infinia design **[7]**. A more recent development by Embraco, is an oil-free linear compressor

designed for R134a and R600a **[8]**. A patent published in 2005 shows a compressor that has significant similarities with the Sunpower design **[9]**. Bradshaw et al. **[10]** have also built a linear compressor model that was validated by testing a prototype linear compressor that used a moving magnet motor designed by H2W Tech.

A number of works have been undertaken to improve the energy efficiency of refrigeration system using traditional reciprocating compressors. Bolaji [11] experimentally evaluated the refrigeration performance by using different refrigerants and demonstrated that R152a can be used as replacement for R134a in domestic refrigerator. A model-based optimization strategy for vapour compression refrigeration cycle was proposed by Zhao et al. [12] to obtain an optimal set point under different operating conditions. Bansal et al. **[13]** reviewed the advantages of linear compressor technologies over traditional crank-drive reciprocating compressors for domestic applications and concluded that linear compressors offer higher efficiency and a more promising alternative to control the refrigeration capacity.

Oxford's role in the development of linear machines started in the late 1970's when there was a requirement to cool an instrument on a satellite designed to investigate the Earth's atmosphere. Since then, there have been three generations of linear compressor developed in the University of Oxford for space applications **[14, 15, 16]**, all of which have a moving coil motor. Outside of space applications, cost has been the major obstacle to extending the use of this technology. This is partly due to the low production numbers, but there also are aspects of the compressor design that are not favourable for low cost mass production. The moving coil linear motor itself has significant engineering challenges that have been discussed by Bailey et al. **[17]**.

1.2 A Moving Magnet Motor Design

Since moving coil compressors are too expensive to be used in many applications, the need for a low cost in materials and manufacture led to a novel low-cost moving magnet linear motor; this is shown in Fig. 1 (a). This moving magnet motor has transverse flux paths between the static part and the moving magnet assembly.

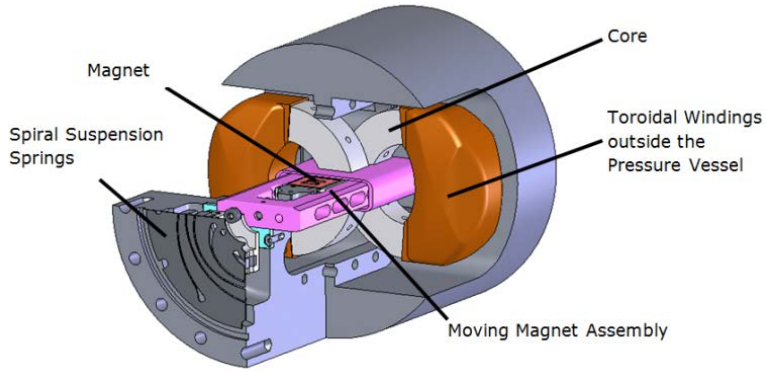

(a) Moving magnet motor design

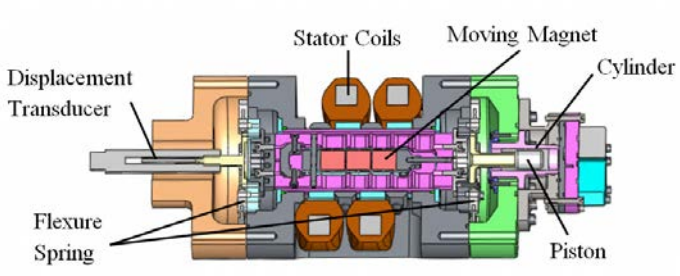

(b) Cross section of the linear compressor and motor

Fig. 1 Design of the 100W Oxford moving magnet compressor

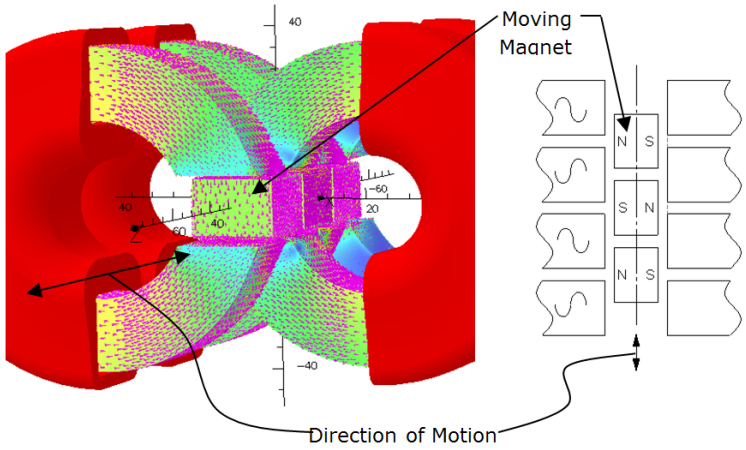

Fig. 2 Magnetic circuit and flux distribution for a design with 4 cores and 3 magnets

The static part of the motor consists of a series of magnetic circuits formed from a coil that is wound around laminated cores, which are slotted to form pole pieces, leaving a rectangular air gap. The cores are positioned so that all the air gaps are aligned along the motor axis. The disposition of neighbouring cores alternates so that the coils do not obstruct each other.

Within this gap is the moving magnet assembly, consisting of a number of rectangular magnets arranged in a line, which occupy the air gap created by the static assembly. The polarisation of the magnets (shown in Fig. 2) alternates and is arranged so as to induce fields that circulate around the adjacent cores. The moving magnet assembly appears to be simple and robust, and the magnet utilisation is good and the moving mass is low. The resistive and core losses can be kept low so that high efficiencies can be achieved.

The Sunpower type moving magnet linear motor, which has been widely adopted, uses a tubular magnet that is cantilevered from the suspension system. The design reported here uses a magnet assembly that is supported at both ends, so there can be greater radial stiffness in the suspension system. In both designs, an alternating electrical current is applied to the (static) wire wound cores, which induces an alternating axial force in the moving magnet assembly. The compressor piston is directly attached to the moving magnet assembly and therefore reciprocates at the same frequency. The piston and cylinder for this compressor are made from stainless steel and the piston has a polymeric coating that was finished by turning; the cylinder bore was ground.

The integration of the motor with the linear suspension system is illustrated in Fig.1 (b). Two sets of spiral springs support a moving magnet assembly attached to the shaft and piston (only one set of springs is visible in Fig. 1). The spiral springs can easily flex (allowing movement) in the axial direction, but have a high radial stiffness, so that the system is constrained to act as a linear bearing. The accuracy of this linear system permits a radial clearance of about 10 μm to be used. This is sufficient to avoid wear, while keeping leakage losses to a minimum. Consequently, the linear suspension system has great longevity, needs no lubrication, and has a high efficiency. The pressure containment is achieved by enclosing the moving magnet assembly in a rectangular tube, which is positioned within the air gap and sealed around both ends into the compressor body. It can be seen that in this design the coil assemblies are outside the pressure vessel as the magnetic circuits are attached externally to the compressor body.

There are two identical compressor 'halves' mounted in line, and the two balanced halves operate in opposite directions from one another to virtually eliminate vibration. The two compressor halves share suction and discharge lines. Further details of the compressor design have already been reported **[17]**.

Table 1 gives the design specifications of the moving magnet compressor. The linear motor was modelled using the Vector Fields FE Magnetic Circuit Analysis software to evaluate its characteristics. At an operating frequency of 50 Hz, a peak motor force of 84 N was predicted, together with a shaft power of 100 W, indicating a motor efficiency of 88% based on an input power of 112 W.

Table 1 Design Specifications for each compressor

Total mass of magnet/piston (kg)	0.66
Piston diameter (mm)	18.99
Total series[1] resistance of coils (Ω)	14
Peak shaft force (N)	84
Peak current at peak force (A)	1.29
Flexure axial stiffness (Total) (kN/m)	17
Maximum stroke (mm)	14

[1]The four motor coils were connected with two coils in series then each pair in parallel to give a resistance of ~3.5 Ω for each compressor half.

2. Linear Compressor Model

The performance of the free-piston linear compressor has been modelled with a lumped parameter model, so as to be able to predict: piston displacement, mass flow rate, temperature and pressures generated inside the cylinder and motor drive case. The reciprocating piston is directly attached to the linear motor. A schematic of the compressor model is shown in Fig. 3.

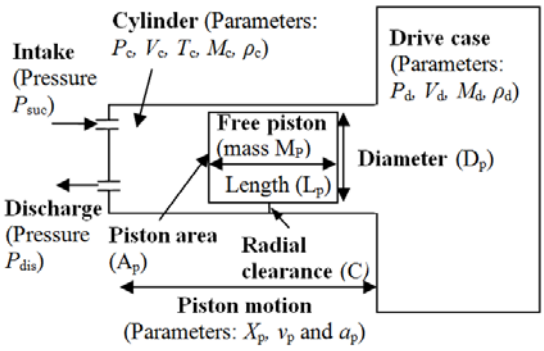

Fig. 3 Schematic defining the key parameters for the free-piston linear compressor model

The forces in the system comprise the motor force F_{motor} (assumed sinusoidal), the spring force F_{spring}, the cylinder gas pressure force F_{cylinder}, the drive case gas pressure (body pressure) force $F_{\mathrm{drivecase}}$, and the damping force (or drag force) due to friction between the cylinder wall and the piston F_{damping}. In effect the piston motion is a forced, damped, simple harmonic oscillator. The resultant force that determines the acceleration and movement of the piston F_{piston} is the sum of the other forces acting on it, as shown in Equation (1).

$$F_{\mathrm{piston}} = F_{\mathrm{motor}} - F_{\mathrm{spring}} - (F_{\mathrm{cylinder}} - F_{\mathrm{drivecase}}) - F_{\mathrm{damping}} \tag{1}$$

In terms of the parameters defined in Fig. 2:

$$\mathrm{M_p} a_{\mathrm{p}} = F_{\max} \cos(2\pi f t) - \mathrm{k} X_{\mathrm{p}} - \left(P_{\mathrm{c}} \mathrm{A_p} - P_{\mathrm{d}} \mathrm{A_p}\right) - \beta v_{\mathrm{p}} \tag{2}$$

The damping coefficient β is readily calculated as the flow in the clearance seal and can be treated as laminar. This represents viscous damping, which has been shown previously in Liang et al. **[1]** to be the only significant form of damping for the piston in the compressor:

$$\beta = \frac{\pi D_{\mathrm{p}} L_{\mathrm{p}} \mu}{C} \tag{3}$$

Equation (2) can be solved to find the piston acceleration a_{p}, and the displacement can then be found numerically. In Equation (3) it is assumed that the clearance is constant, while in reality it is likely to be variable and indeed the piston can be eccentric within the cylinder. However, as this term is very small, then this assumption is not important.

From the displacement, new volumes, pressures and gas densities for the cylinder and drive case can be calculated, along with other effects such as mass leakage past the piston, between the cylinder and drive case:

$$\dot{m}_{\mathrm{leak}} = \frac{\pi \mathrm{D_p} C^3 (P_{\mathrm{c}} + P_{\mathrm{d}})}{24 \mu L_{\mathrm{p}} R T_{\mathrm{leak}}} (P_{\mathrm{c}} - P_{\mathrm{d}}) \tag{4}$$

The internal energy change of the system can be calculated for each time step as:

$$\frac{\Delta U}{\Delta t} = \dot{Q} - \dot{W} - \dot{m}_{\mathrm{leak}} h_{\mathrm{leak}} + \dot{m}_{\mathrm{suc}} h_{\mathrm{suc}} - \dot{m}_{\mathrm{dis}} h_{\mathrm{dis}} \tag{5}$$

Solution of $\dot{Q}$ requires the rate of heat transfer between the compressed gas and the cylinder wall, and this was calculated using the Fagotti and Prata correlation **[18]**. This correlation accounts for instantaneous heat transfer between the bulk fluid and the cylinder walls during the compression process, which is an important factor influencing the performance of reciprocating compressors. Heat is transferred from the bulk fluid to the cylinder wall during the compression process and then transferred back from the cylinder wall to the fluid during the expansion process. This heating of the fluid in the cylinder during expansion limits the rate at which fluid enters the cylinder via the suction valve and thereby influences the overall mass flow rate. A key parameter governing this process is the cylinder wall temperature, which was assumed to be constant for the purposes of the present model. It was assumed to be an average of the maximum discharge temperature predicted (i.e. 120ºC) and the suction temperature (i.e. 20ºC), and therefore a value of 70ºC was assumed throughout. Equation (5) can then be solved numerically to give the cylinder gas pressure; full details of the procedure are in Davies et al. **[19]**.

3. Experiments

3.1 Experimental Setup

The compressor has been designed for a refrigeration system and the test rig was established for future tests with refrigerant. To provide baseline experimental data, measurements were first carried out using nitrogen. The gas selection (nitrogen or helium) had a negligible effect on the compressor performance.

Fig. 4 shows the linear compressor test schematic that is also suitable for use with refrigerants. The hot and pressurised gas from compression in the cylinder is discharged into a heat exchanger (condenser). A needle valve (main flow valve) controls the pressure ratio, and this is followed by another heat exchanger with a heater that would act as an evaporator. The bleed valve controls pressure in the compressor body so as to maintain the correct mean piston position. The piston displacements are measured by LVDTs.

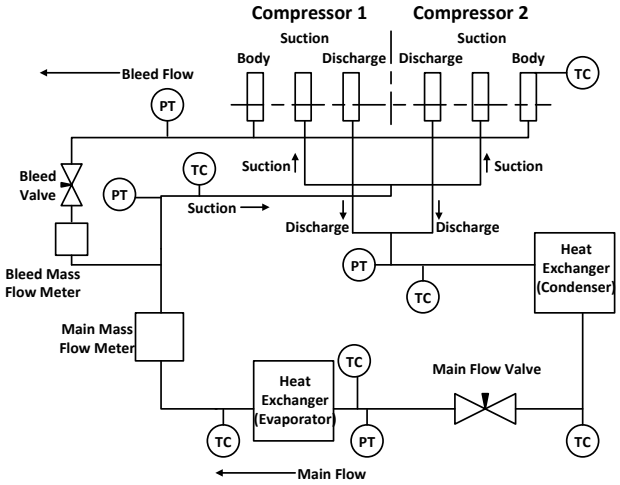

Fig. 4 Linear compressor test loop (TC – thermocouple, PT – pressure transducer)|

During compressor operation, the drive frequency from a signal generator is adjusted to maintain resonance and the piston stroke (Peak-to-Peak value from an oscilloscope) is set by a voltage amplitude control. A power amplifier amplifies the analogue signal in order to drive the linear compressor. A capacitance box is employed to permit adjustment of the capacitance in response to different resonant frequencies (this power factor correction reduces the voltage requirement for the amplifier). The power input, overall RMS current and voltage can be read and manually recorded from a power meter in addition to logging the current and voltage on a high speed data acquisition system.

3.2 Experimental Method

The prototype linear compressor was operated under resonance with different strokes at various constant pressure ratios using nitrogen. The bleed valve and main valve (shown in Fig. 4) were adjusted to keep the pressure ratio constant and the mean position of the piston constant. The resonant frequency is measured by changing the drive frequency of the function generator and changing the amplifier gain to keep the stroke constant – resonance was assumed to be the frequency at which the power input is a minimum for the specified stroke.

The specific test conditions using nitrogen are shown in Table 2. Prior to operation, the compressor was filled with gas to a 'fill pressure', and this defined the nominal mean pressure in the operating system. The two compressor halves are nominally identical, but due to the varying DC offset of the piston and for reasons of safety (not hitting the cylinder head), the maximum stroke used was limited to 13 mm.

Table 2 Experimental conditions

Gas	nitrogen
Pressure ratio	1.5, 2.0, 2.5, 3.0, 3.5
Stroke (mm)	6, 8, 10, 11, 12, 13
Fill pressure, absolute (bar)	3.5, 7, 8

4. Results and Discussion

Among those test conditions shown in Table 2, five typical ones are considered in the model to predict the compressor performance as comparisons with the experimental data. The selected operation conditions (operation frequency, suction and discharge pressures, fill pressure), together with the key performance parameters from the linear compressor measurements are shown in Table 3.

Table 3 Results from Tests of the Prototype Linear Compressor (one half)

Test No.	1	2	3	4	5
Fill pressure (bar)			7		
Operation frequency (Hz)	33.5	32.5	35	35	36.5
Suction pressure (bar)	4.96	5.01	4.37	4.40	3.86
Discharge pressure (bar)	9.94	10.02	10.95	11.01	11.60
Stroke (mm)	12.4	13.5	12.4	13.5	13.4
Mass flow rate (g/s)	0.55	0.62	0.44	0.51	0.43
Shaft power (W)	48	54	53	62	63

4.1 Inferred Cylinder Pressure from Measurements

Parameters from experiments can be used to calculate the P-V diagram. The cylinder gas pressure force can be inferred from Equation (1) as

$$F_{\text{cylinder}} = F_{\text{motor}} - F_{\text{piston}} - F_{\text{spring}} - F_{\text{damping}} + F_{\text{drivecase}} \tag{6}$$

This can be expanded further to give:

$$P_{\text{c}} = (F_{\text{motor}} - \text{M}_{\text{p}} a_{\text{p}} - \text{k}_{\text{s}} X_{\text{p}} - \beta v_{\text{p}})/\text{A}_{\text{p}} + P_{\text{d}} \tag{7}$$

Let the motor (shaft) force be a function of measured current and armature position (piston displacement)

$$F_{\text{motor}} = B(X_{\text{p}})I \tag{8}$$

which has been calibrated into a 3-D map (force-current-displacement) so that the shaft force can be retrieved with interpolation for each operating point. If an effective stiffness was being computed so as to estimate the resonant frequency, then the contribution from the cylinder pressure would be included as well as the mechanical spring stiffness.

As has been mentioned above, the piston displacement X_{p}, input current I and drive case pressure P_{d} are measured. Therefore, using Equation (7), the cylinder pressure can be derived for each test condition.

Fig. 5 gives the results for interpolation of the shaft force using inputs of the measured current and displacement, along with the measured body pressure (drive case gas pressure) for the test condition with a stroke of 13 mm and pressure ratio of 3.0. The peak force is about 91.7 N, and this agrees well with value predicted in **[17]**. Both vary nearly sinusoidally, indicating a possible sinusoidal cylinder pressure variation during compression and expansion if there was no flow.

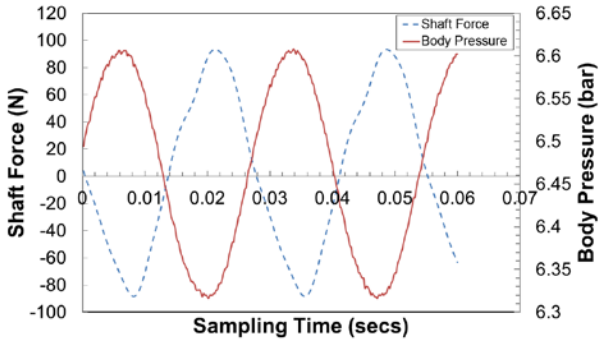

Fig. 5 Interpolated shaft force and measured body pressure for a stroke of 13 mm and a pressure ratio of 3.0 when the compressor is filled to an initial pressure of 7 bar

Fig. 6 compares the calculations of the cylinder pressure between the model and measurement in approximately two thermodynamic cycles for the design point. The maximum cylinder pressures are 12.20 bar and 12.44 bar from the model and measurement respectively, indicating a discrepancy of 1.9%. The minimum cylinder pressures are 3.81 bar and 3.05 bar respectively and the discrepancy is about 18.0%. It can be seen that during the compression and expansion processes, the model and measurement agree well with each other, while during the discharge and suction processes, the calculations are slightly different. The reason for the difference in calculation during the discharge and suction processes is because the compressor model uses a simple model for the two valves which are employed to control the flow of fluid into and out of the compressor. A more realistic representation of the effects of the reed valves will provide a more accurate simulation of restrictions within the flow path. The detailed opening and closing of the two valves will be shown in the next section.

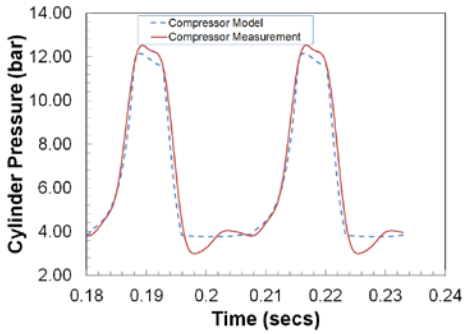

Fig. 6 Comparison of calculations of cylinder pressure between compressor model and measurement for a stroke of 13 mm and a pressure ratio of 3.0, test condition 5 in Table 3

4.2 Valves Opening and Closing

The measured piston displacement and its acceleration (the second derivative of the displacement) are plotted together with the derived cylinder pressure for approximately two cycles in Fig. 7. Note that positive displacement means piston movement away from the cylinder head. From this graph, the

opening and closing of the suction and discharge valves can be identified, and so the four thermodynamic processes can be separated.

At point A, the suction valve closes and the piston moves towards the cylinder head to compress the gas. The cylinder pressure follows an approximately sinusoidal pattern during the compression process because of the sinusoidal acceleration as both the valves are closed. From A to B is the compression process.

When the cylinder pressure rises to point B (about 12.2 bar), the discharge valve opens (the cylinder pressure is higher than the discharge pressure) and the acceleration reduces. The compression volume is still decreasing and the cylinder pressure rises up to 12.52 bar until the reed valve fully opens. The discharge valve closes at point C and the cylinder pressure (at 11.9 bar) is lower than the discharge pressure. This is the discharge process.

From point C to point D (both valves are closed), and the compressor is undergoing an expansion process and there is no mass transfer; the cylinder pressure varies approximately sinusoidally and the piston decelerates.

When the cylinder pressure drops to 3.9 bar, which is below the suction pressure, the suction reed valve opens. The cylinder pressure keeps reducing until the valve fully opens. The minimum cylinder pressure is 3.1 bar. As the valve lift increases, more mass is transferred into the cylinder. The suction process ends at point E where the suction valve fully closes. It is shown that the suction process (D-E) is significantly longer than discharge process (B-C). This is because the mass of gas transferred in and out the cylinder must be the same for stable operation of the compressor, and as the density of the gas during suction is much lower than during discharge, the volume flow rate must be higher.

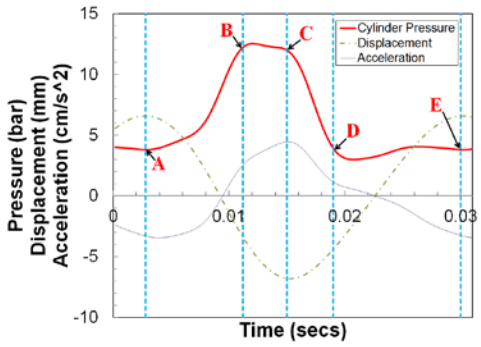

Fig. 7 Cylinder pressure, piston displacement and acceleration for a stroke of 13 mm and a pressure ratio of 3.0, test condition 5 in Table 2

4.3 P-V Loop

As described in section 4.1, the cylinder pressure can be calculated from measurements of the piston displacement, the body pressure, and current (using the motor force characteristics). The cylinder volume is derived from the cylinder dimensions and piston displacement. Using the compressor model (from section 2) a diagram of cylinder pressure as a function of cylinder volume (P-V loop) can be derived for each operational condition.

Fig. 8 compares the experimentally derived P-V loop with the compressor model, together with the measured discharge and suction pressures for a stroke of 13 mm and a pressure ratio of 3.0. It is worth emphasising that the suction and delivery pressures were not used in deriving the cylinder pressure, so

these provide useful corroboration of the cylinder pressure. Overall, the two P-V loops follow a very similar pattern for each cycle (also predicted in Fig. 6), particularly in the process of compression. It is also seen that the compressor model gives a better representation of the discharge valve behaviour, compared to the suction valve. During the suction process, the compressor cylinder pressure falls below the suction line pressure. Although the opening and closing for the two valves look slightly different between the model and the measurements, the measured cylinder pressures at each opening or closing point for the valves agrees with the model.

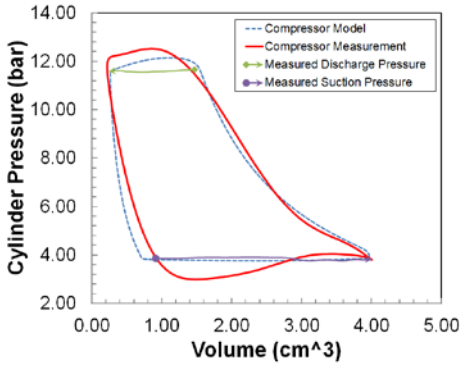

Fig. 8 Derived P-V loop compared with the compressor model at the design point (a stroke of 13 mm and a pressure ratio of 3.0, test condition 5 in Table 3)

The accuracy of the experimentally derived P-V loop and the model prediction can be further demonstrated by a comparison at another operational condition (a stroke of 13 mm and a pressure ratio of 2.0). Fig. 9 shows the comparison along with the measured discharge and suction pressures.

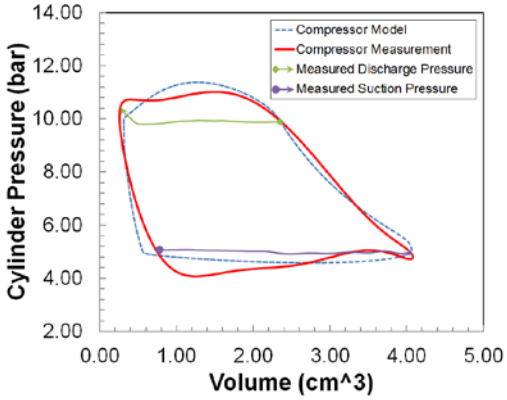

Fig. 9 P-V loop comparison between model and measurement for a stroke of 13 mm and a pressure ratio of 2.0, test condition 2 in Table 3

4.4 Measured Compressor Performance

Fig. 10 plots the motor efficiency (the ratio of shaft power to input power) against the input power for four different pressure ratios (PR). The motor efficiency decreases as the input power increases, mainly because the copper loss (*I* squared *R* loss) dominates over the shaft power increase with the current. At a low input power (32 W), the motor efficiency can be ~ 89%. In addition, for the same input power, the motor efficiency increases with a rising pressure ratio due to the increasing resonant frequency. For the design point (stroke of 13 mm and PR 3.0), the compressor operates at 36.5 Hz with an input power of 177.2 W; the motor efficiency is approximately 74%. This compares with Bradshaw et al. **[2]** who used a commercial moving magnet linear motor from H2W which has a

much lower motor efficiency of 40%. Unger et al. **[5]** introduced a compact moving magnet linear compressor for CPU cooling and their motor efficiency was 80%-90% for a power input ranging from 100 W to 200 W. Possamai et al. **[20]** designed a compact refrigeration system for laptop cooling using a moving magnet linear compressor designed by Embraco with a motor efficiency of 71%. Tests on a hermetically sealed refrigeration compressor that used an induction motor showed that the motor efficiency increased from about 20% to 60% as the load increased, since the magnetic losses are high and are mostly independent of the power output.

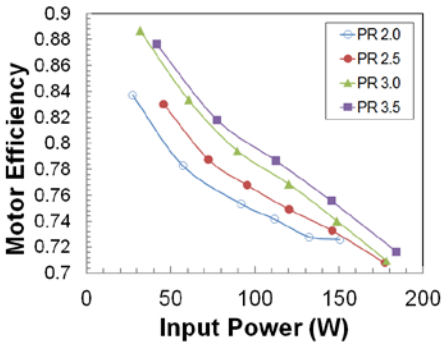

Fig. 10 Motor efficiency against input power for different pressure ratio

Overall efficiency (ideal adiabatic or isothermal thermodynamic power divided by the input electrical power) is given in Fig. 11 for tests with the same stroke (13 mm). Both the adiabatic and isothermal efficiencies show a similar trend with an increasing pressure ratio; the adiabatic efficiency is of course always higher than the isothermal efficiency. The higher pressure ratio leads to an increased seal leakage loss, and pressure drop. Within the operating range, the maximum adiabatic efficiency is about 60% and the isothermal efficiency is 56%. The overall efficiencies for the design point (stroke of 13 mm and pressure ratio of 3.0) are an adiabatic efficiency of 54% and an isothermal efficiency of 46%.

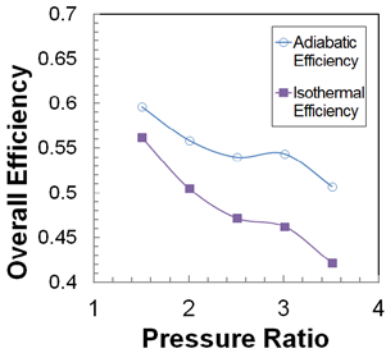

Fig. 11 Overall efficiency as a function of pressure ratio for an operating stroke of 13 mm

Experiments have been carried out for different fill pressures of 3.5 bar, 7.0 bar and 8.0 bar. Fig. 12 shows the motor efficiency and overall efficiency for the different fill pressures. It can be seen that a lower fill pressure leads to a higher motor efficiency. This is because the lower fill pressure requires less input current for the same stroke, so there is less copper loss (I^2R). In general, the overall adiabatic and isothermal efficiencies rise as fill pressure decreases for the same stroke. However, to obtain high-pressure compressed gas, the compressor needs to be operated at a certain fill pressure at which the performance will still be efficient. This linear compressor is designed for a fill pressure of 7 bar.

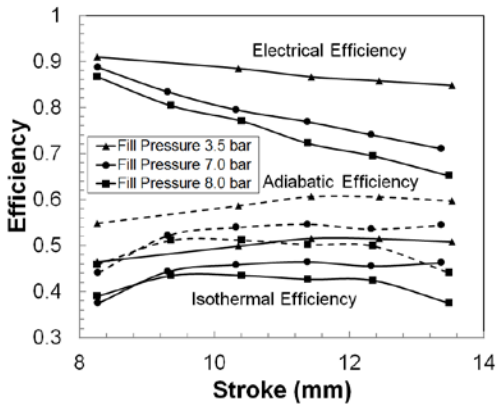

Fig. 12 Compressor efficiency (pressure ratio of 3.0) when operated at different fill pressures

Fig. 13 gives an alternative efficiency comparison for different fill pressures when operating at a pressure ratio of 3.0. The thermodynamic efficiency is defined as the ratio of the thermodynamic power (either adiabatic or isothermal) to the shaft power. It is shown that thermodynamic efficiency generally increases with stroke and appears to be very similar for different fill pressures at the same stroke. This is mainly because the thermodynamic losses (principally heat transfer, seal leakage, and valve pressure drops) are more determined by the pressure ratio than the mean pressure in the drive case (the body pressure). When the compressor operates at a stroke of 13 mm, a pressure ratio of 3.0 and a fill pressure of 7.0 bar, the adiabatic and isothermal thermodynamic efficiencies are 77% and 66% respectively.

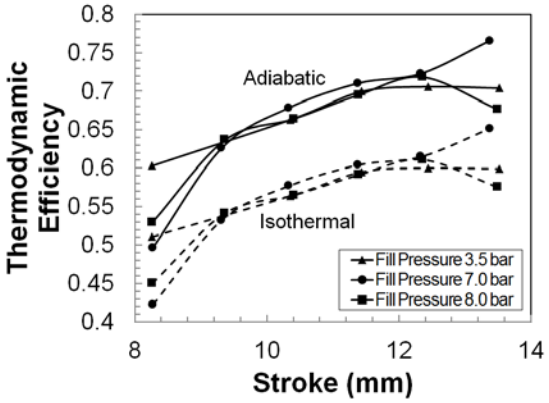

Fig. 13 Thermodynamic efficiency for operation with a pressure ratio of 3.0 for different fill pressures

4.5 Model Validation

Comparisons of predicted and measured data for all 5 test conditions in Table 3 are shown in Figs 14 to 16 below.

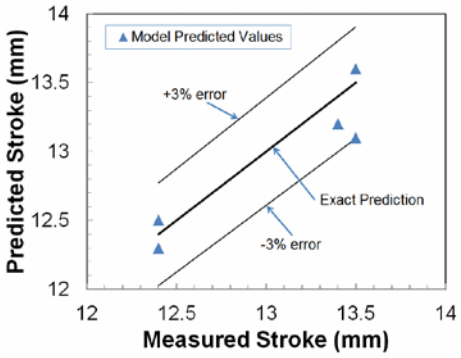

Fig. 14 Predicted and measured stroke lengths for test conditions 1-5, as defined in Table 3

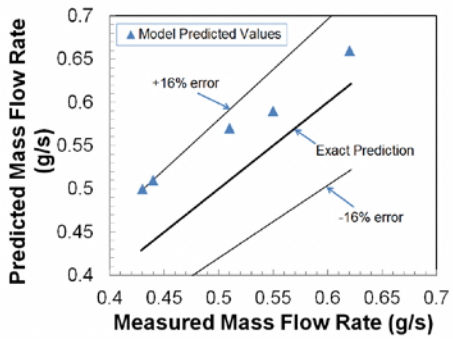

Fig. 15 Predicted and measured mass flow rates for test conditions 1-5, as defined in Table 3

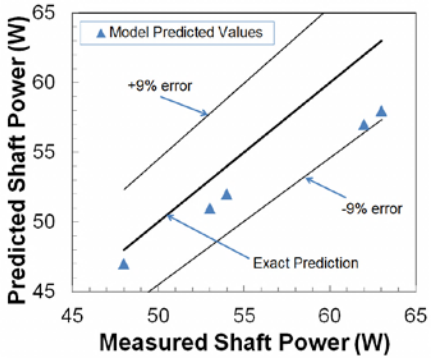

Fig. 16 Predicted and measured shaft powers for test conditions 1-5, as defined in Table 3

The comparison of the predicted piston stroke lengths with the experimentally measured values in Fig. 14 shows agreement within 3% of the measured values. The average mass flow rates predicted also showed good agreement with the experimental values, with a maximum difference of 16%, as shown in Fig. 15, with the measured mass flow rate always being less than that predicted by the model. Fig. 16 shows that shaft power values are in reasonable agreement with the measured values (within 9%). In each case the shaft power values were under predicted by the model, and this could be attributed to valve leakage and heat transfer effects. The re-absorption of heat from the cylinder walls during expansion appears to be a critical element in correlating the shaft power and the mass flow rate. At lower cylinder wall temperatures (i.e. less than the assumed average temperature of 70ºC), the over prediction of the mass flow rate and under prediction of shaft power by the model relative to experimentally measured values increased, while at higher temperatures, closer agreement between predicted and measured values was achieved. Cylinder discharge temperatures predicted from the model were generally of the order 110 to 120ºC.

4.6 Compressor Losses

A simplified analysis of the linear compressor losses is given in Fig. 17. The diagram separates the compressor losses into two terms, electrical losses (or motor losses) and thermodynamic losses. The motor loss is composed of mainly the copper loss, core loss (hysteresis loss and eddy current loss) and other losses (i.e. additional eddy current losses). These losses will account for power lost in the moving magnet motor. The shaft power generated will be driving the piston backwards and forwards. The thermodynamic losses stem from seal leakage, heat transferred (out during compression and in during expansion) and pressure drops across the valves. Most of the loss processes present here have been characterized by measurements and analysis (valve leakage can be ignored as this was tested strictly prior to the dynamic measurements). A systematic analysis on these losses will be sufficient to account for the motor efficiency and overall efficiencies calculated in Fig. 12. Understanding and reducing these loss mechanisms is the key to producing a more efficient linear compressor for future use.

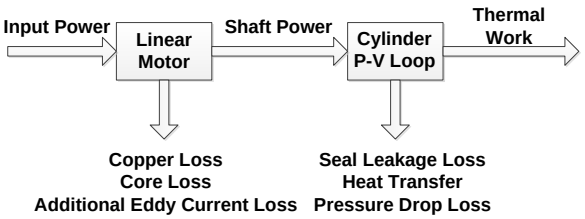

Fig. 17 Schematic of linear compressor losses (simplified)

Based on the P-V diagram at the design point in Fig. 8, the area enclosed by the P-V loop is calculated as the net power (net work over cycle time), to give 62.1 W and 62.8 W for the two compressor halves. The total net power calculated (124.9 W) is very close to the shaft power (125.8 W) by using the interpolated shaft force (Fig. 5).

For the design point, copper loss amounts to 25.8 W and the total core loss is approximately 3 W from **[21]**, including the eddy current loss within the core. However, there were two other eddy current losses occurring in the compressor pressure containment tube and the aluminium body. Both of these losses are very significant (estimated as 5 W and 10 W for the design point at 36.5 Hz). Since the additional eddy current losses can be reduced, the motor efficiency with a revised design would be higher than in Fig. 12 (approximately 86%). Fig. 18 summarizes the major parts of the compressor losses. The copper loss is responsible for about 34% of the reduction in compressor efficiency. The pressure drop loss across the valves is calculated from Fig. 8 (the area enclosed by the discharge process curve in the P-V loop and the measured discharge pressure, plus the area enclosed by the suction process curve and the measured suction pressure) as 23 W (27%). The heat transfer loss is inferred by difference, and represents about 13% of the total losses.

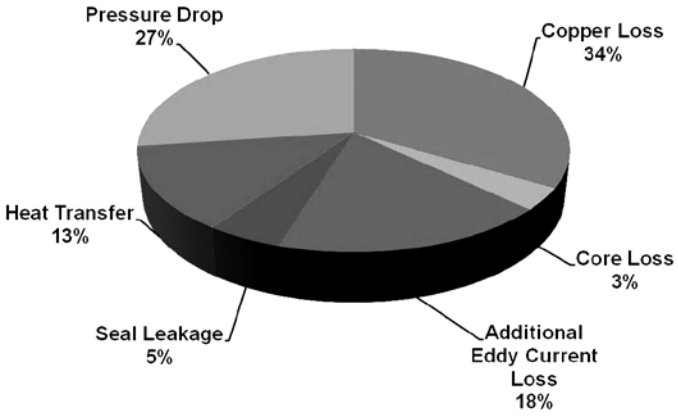

Fig. 18 Distributions of the compressor losses for the design point, test condition 5, Table 3

5. Conclusions

A 1-D mathematical model has been built to predict the performance of a moving magnet linear compressor. Performance of a prototype linear compressor was measured in a test rig using nitrogen gas to be compared with the modelling results.

(1) The inferred cylinder gas pressure from measurements demonstrates the valves opening and closing very clearly. P-V loops from measurements and model agree well with each other. A more realistic valve model would improve the agreement further.
(2) Close agreement between the model and measurements have also been found in other performance parameters, e.g. mass flow rate, stroke length and shaft power. This will enable the model to be employed for a detailed sensitivity analysis and further developments in the design of linear compressors.
(3) Experimental data shows that the prototype linear compressor can achieve a motor efficiency of 74% at the design point. The motor efficiency can be improved to be over 86% with a revised motor design (to reduce the additional eddy current losses).
(4) For the design operation point, the seal leakage loss in the linear compressor represents 5% while pressure drop loss is responsible for 27%. The most significant loss in the motor is the copper loss, which will reduce the motor efficiency as the input power increases.

6. Acknowledgements

The authors acknowledge The Engineering and Physical Sciences Research Council (EPSRC) for funding the construction of the linear compressor.

NOMENCLATURE

1-D	one dimensional
3-D	three dimensional
A	area (mm^2)
a	acceleration ($mm\ s^{-1}$)
B	magnetic flux density (T)
C	clearance (μm)
D	diameter (mm)
DC	direct current
F	force (N)
f	frequency (Hz)

FE	finite element
h	enthalpy (kJ kg^{-1})
I	current (A)
k	spring constant (N mm^{-1})
L	length (mm)
LVDT	linear variable differential transformer
M	mass (g)
$\dot{m}$	mass flow rate (g s^{-1})
P	pressure (bar)
PT	pressure transducer
PR	pressure ratio
$\dot{Q}$	heat gain (W)
R	specific gas constant (J kg^{-1} K^{-1})
RMS	root mean square
t	model run time (s)
TC	thermocouple
ΔU	change in internal energy (J)
V	volume (mm^3)
v	velocity (mm s^{-1})
$\dot{W}$	rate of compression work (W)
X	displacement (mm)

Greek

β	damping coefficient (N s m^{-1})
μ	dynamic viscosity (Pa s)
ρ	density (kg m^{-3})

Subscripts

c	cylinder
d	drive case
dis	discharge
leak	leakage across clearance seal
p	piston
s	spring
suc	suction

References

[1] **Liang, K., Dadd, M.W.,** and **Bailey, P.B.** Clearance seal compressors with linear motor drive – part i: background and system analysis. *Proc. IMechE, Part A: Journal of Power and Energy*, 2013, 227(3), pp. 242-251.

[2] **Bradshaw, C.R., Groll, E.A.,** and **Garimella, S.V.** A comprehensive model of miniature-scale linear compressor for electronics cooling. *Int. J. Refrigeration*, 2011, 34, pp. 63-73.

[3] **Bailey, P.B., Dadd, M.W.,** and **Stone, C.R.** Cool and straight: linear compressors for refrigeration. *Proc. Inst. Refrigeration*, 2010-11, 4-1.

[4] **Van der Walt, N.R.,** and **Unger, R.** Linear compressors – a maturing technology, Sunpower Inc, Athens, Ohio, USA, 1994. http://www.sunpower.com/library/pdf/publications/Doc0054.pdf. (accessed 25/11/2012)

[5]Many Sunpower papers are available at http://www.sunpower.com/library/coolingcompression.php. (accessed 25/11/2012)

[6] **Yarr, G. A.,** and **Corey, J. A**. Linear electrodynamic machine, *US Patent* 5389844, 1995.

[7] **Nasar, S. A.,** and **Boldea, I.** Linear electrodynamic machine and method of making and using same. *US Patent*, 5654596, 1997.
[8] http://www.acr-news.com/news/news.asp?id=2231. (accessed 25/11/2012)
[9] **Lilie, D. E. B.** Reciprocating compressor driven by a linear motor. *US Patent*, No. 7316547 B2, 2008.
[10] **Bradshaw, C.R.** A miniature-scale linear compressor for electronics cooling. *Ph.D. Thesis*, Purdue University, 2012.
[11] Bolaji, B.O. Experimental study of R152a and R32 to replace R134a in a domestic refrigerator. *Energy*, 2010, 35, pp. 3793-3798.
[12] Zhao, L., Cai, W.-J., Ding, X.-D., and Chang, W.-C. Model-based optimization for vapor compression refrigeration cycle. Energy, 2013, 55, pp. 392-402.
[13] **Bansal, P., Vineyard, E.,** and **Abdelaziz, O.** Advances in household appliances – a review. *Applied Thermal Engineering*, 2011, 31, pp. 3748-3760.
[14] **Bradshaw, T.W., Delderfield, J., Werret, S.T.,** and **Davey, G.** Performance of the Oxford miniature Stirling cycle refrigerator. *Advances in Cryogenic Engineering, Plenum,* 1986, **31**, 801-809.
[15] **Davey, G.** Review of the Oxford cryocooler. *Advances in Cryogenic Engineering, Plenum*, 1990, **35 B**, pp. 1423-1430.
[16] **Bailey, P.B., Dadd, M.W., Hill, N., Cheuk, C.F., Raab, J.,** and **Tward, E.** High performance flight cryocooler compressor. *Cryocoolers 11,* Kluwer Academic/Plenum Press, New York 2001, pp. 169-174.
[17] **Bailey, P.B., Dadd, M.W.,** and **Stone, C.R.** An oil-free linear compressor for use with compact heat exchangers. *Proc. Intl. Conf. on Compressors and their Systems, IMechE*, London, 2009, pp. 259-268.
[18] **Fagotti, F.,** and **Prata, A.** A new correlation for instantaneous heat transfer between gas and cylinder in reciprocating compressors. *Proc. Intl. Compressor Engineering Conf.*, Purdue University, West Lafayette, IN, USA, 1998, pp. 871-876.
[19] **Davies, G.F., Eames, I.W., Bailey, P.B, Dadd, M.W., Janiszewski, A., Stone, C.R., Maidment, G.G.,** and **Agnew, B.** Cooling microprocessors using vapour compression refrigeration. *Proceedings of the 12th IEEE Intersociety Conference on Thermal and Thermomechanical Phenomena in Electronics Systems (ITherm).* Institute of Electrical and Electronics Engineers (IEEE), Piscataway, N.J., USA, pp. 1-8.
[20] **Possamai, F., Lilie, D.E.B., Zimmermann, A.J.P., and Mongia, R.** Miniature vapour compression system. *Proc. Intl. Compressor Engineering Conf.*, Purdue University, West Lafayette, IN, USA, 2008, 2392, pp. 1-8.
[21] Cogent Power Ltd . *Electrical steel grain oriented Unisil*, Unisil-H, 18.